Quasi-2D FCC lithium crystals inside defective bi-layer graphene: insights from first-principles calculations

Zhang, X.; Ghorbani Asl, M.; Zhang, Y.; Krasheninnikov, A.;

Originally published:

April 2023

Materials Today Energy 34(2023), 101293

DOI: https://doi.org/10.1016/j.mtener.2023.101293

Perma-Link to Publication Repository of HZDR:

https://www.hzdr.de/publications/Publ-36733

Quasi-2D FCC lithium crystals inside defective bi-layer graphene: insights from first-principles calculations

Xuemei Zhang,[a,b,] Mahdi Ghorbani-Asl,[a]* Yongsheng Zhang,[c] and Arkady V. Krasheninnikov[a,d] *

[a] Institute of Ion Beam Physics and Materials Research, Helmholtz-Zentrum Dresden-Rossendorf, D-01328, Dresden, Germany

[b] Science Island Branch of Graduate School, University of Science and Technology of China, Hefei 230026, China

[c]Advanced Research Institute of Multidisciplinary Sciences, Qufu Normal University, Qufu, Shandong Province, 273165, China

[d] Department of Applied Physics, Aalto University, P.O. Box 11100, 00076 Aalto, Finland

Abstract

Quasi-2D crystals inside bilayer graphene have been observed in in-situ TEM experiments [Nature 564 (2018) 234]. It was also revealed that Li crystals have the FCC structure, nucleate at point defects in graphene and contain impurity atoms. Using first-principles calculations, we systematically study the interaction of isolated Li atoms and those assembled in FCC crystals with vacancy-type defects in graphene and show that quasi-2D Li crystals encapsulated between graphene sheets must indeed nucleate at the defects and that the interaction of not only isolated Li atoms, but also Li crystals with the defects in graphene is strong. We further demonstrate that a moiré pattern develops at the graphene/Li interface. Finally, we investigate the behavior of impurities most likely to be found in the encapsulated Li crystals, such as O, N, S and F and show that all impurity atoms take octahedral interstitial positions and strongly interact with atoms in Li crystals, thus impeding the de-lithiation process. Our theoretical work focused on the fundamental aspects of the behavior of Li inside bilayer graphene should help rationalize the results of in-situ TEM experiments and shed light on the role of impurities in the degradation of anode materials during Li-ion battery operation.

Keywords: Li intercalation, graphene, defects, first-principles calculations

1. Introduction

The operation of the state-of-the-art alkali-metal-ion batteries[1-4] is based on the reversible intercalation of the ions into sp^2-hybridized carbon structures, so that the interaction of alkali-metal atoms with graphitic hosts and the electrochemistry of intercalation compounds have recently been one of the most important topics in materials science. Moreover, the efficient intercalation has been demonstrated to be of pivotal importance for not only energy storage[5-8], but also tuning the opto-electronic properties of bulk[9] and nano-structured layered materials[10-13]. As for the latter, the intercalation of Li atoms into vertical heterostructures assembled from individual sheets of graphene and transition metal dichalcogenides, such as MoS_2, which are also considered as perspective anode materials[14-17], have been studied.

Very recently, lots of attention has been paid to the intercalation of various species into bi-layer graphene (BLG) [8, 11, 12, 18-22], as the robustness of graphene sheets and their stability under electron beam made it possible to investigate[23] the new quasi-two-dimensional (q-2D) materials with atomic resolution using transmission electron microscopy (TEM). In particular, in-situ TEM studies showed the unexpected formation of multi-layer close-packed Li phases between graphene sheets[18] when Li atoms are driven into BLG. Follow-up studies[24] demonstrated that upon lithiation many Li islands with triangular shapes appear simultaneously, presumably due to the predominant nucleation of Li structures at vacancy-type defects in graphene. We note that the formation of Li clusters in graphene-based systems has been previously discussed[25, 26] in connection with Li dendrites formation, which is associated with battery degradation.

The observed q-2D Li crystals had FCC lattices and consisted of 3-9 closely packed (111) planes of Li atoms. The presence of impurity atoms (mostly oxygen) in interstitial positions in the Li crystals was detected, and it was also found that upon delithiation,

the impurities played an important role preventing complete delithiation and giving rise to the formation of amorphous Li-containing compounds.

These observations give rise to several questions concerning the interaction of Li atoms with defects in graphene and impurity atoms. Although it is intuitively clear that isolated Li atoms will interact more strongly with dangling bond atoms in graphene than with pristine graphene, this does not necessarily mean that the growing Li crystals will remain pinned by the defect. Moreover, vacancy-type defects in graphene are known to reconstruct by bond rotations[27, 28], which should decrease the reactivity of defective graphene. In general, the atomic structure of graphene at the interface with FCC Li crystals has not been investigated before. It is not clear either where impurity atoms, such as ubiquitous O, N, etc. would prefer to be, in the bulk of Li crystals or between graphene sheets and Li surface.

Here we employ first-principles calculations to address these issues. By systematically studying the interaction of isolated Li atoms and those in FCC crystals with defects in graphene, we obtain insights into the behavior of q-2D Li crystals encapsulated between defective graphene sheets. Our results also shed light on the energetics of intercalated Li atoms and their agglomeration in the presence of defects. We further investigate the behavior of typical impurity atoms in bulk and q-2D Li crystals.

2. Computational methods

Spin-polarized density functional theory (DFT) calculations were performed using Vienna Ab initio Simulation Package (VASP) [29, 30], based on the plane-wave projector augmented-wave (PAW) method[31]. The exchange-correlation functional was employed in the generalized gradient approximation of Perdew-Burke-Ernzerhof (GGA-PBE)[32]. The Grimme (DFT-D3) method was considered for treating van der Waals (vdW) interactions[33-35]. An energy cut-off of 600 eV for plane-wave expansion was used for the primitive cell (the total energy was converged within 10^{-5} eV) and 400 eV for supercell calculations, respectively. This value of cutoff converged

the defect formation energies and all other relevant quantities within an accuracy of 0.05 eV, which is sufficient for our purpose and made it possible to avoid excessive consumption of CPU time. Various initial configurations of Li atoms on monolayer and between bilayer graphene sheets (AA and AB stacked) were investigated to screen out the most stable configurations. The simulation models of graphene/Li (111) interface were constructed using 10 × 10 graphene supercell on top of a (111) 8 × 8 Li slab, with a total strain of ~0.47%, containing 392 atoms. The Brillouin zone of the primitive cells and supercells were sampled using (12 × 12 × 1) and (4 × 4 × 1) Monkhorst−Pack k-point, respectively[36]. All structures are fully optimized until the maximum force on each atom is less than 0.01 eV/Å. The behavior of impurity atoms in bulk Li crystals were studied by calculating their energetics in a periodic supercell composed of 576 Li atoms. The VESTA[37] and VMD[38] packages were used for visualizing the atomic structures and charge density differences. The isovalue for rendering the isosurfaces is 0.001 e/a_0^3.

The stability of a Li structure in BLG was evaluated by calculating its formation energy E_f as follows:

$$E_f = (E_{\mathrm{Gr+Li}} - E_{\mathrm{Gr}} - \sum_i n_i\mu_i)/\, n_i \quad (1)$$

where $E_{\mathrm{Gr+Li}}$ and E_{Gr} are the energies of the graphene supercell with and without Li atoms, respectively. n_i and μ_i refer to the number of Li atoms and their chemical potential in the bulk elemental phase. It was assumed that for all Li atoms μ_i is the same as in the bulk FCC phase.

To get more insight into the behavior of Li atoms in defective graphene, we also calculated the energy difference ΔE_f between configurations corresponding to all Li atoms located near the defect and in the pristine areas, which is defined as

$$\Delta E_f = E_f^{def}(n_i\mathrm{Li}) - [E_f^{def}\big((n_i - 1)\mathrm{Li}\big) + E_f^{pristine}(1\mathrm{Li})], \quad (2)$$

where E_f^{def} and $E_f^{pristine}$ are the formation energies of the configurations with Li atoms adsorbed on defective and pristine graphene, respectively. It is assumed that one Li atom is always attached to the defect. The sign of ΔE_f indicates if the atoms prefer to cluster on the defect or remain spatially separated.

To analyze the charge transfer between adsorbed Li and graphene, the charge density difference was calculated as

$$\Delta\rho = \rho_{\mathrm{Li+G}} - [\rho_{\mathrm{Li}} + \rho_{\mathrm{G}}] \quad (3)$$

where $\rho_{\mathrm{Li+G}}$ denotes the electronic charge density of the combined system (graphene and Li), and ρ_{Li} and ρ_{G} represent the charge density of the isolated Li subsystem and graphene, respectively.

3. Results and discussion

3.1. Interaction of individual Li atoms with graphene

3.1.1. Interaction of Li atoms with single layer graphene

The TEM in-situ experiments[24] clearly indicated that Li crystals nucleate in the areas of BLG where point defects are present. These defects are likely the vacancies which appeared due to the effects of the electron beam, so that we concentrate on the interaction of Li atoms with vacancies in BLG.

For the sake of completeness, and to establish the link to the results of previous calculations [39, 40], we studied first the interaction of Li atoms with pristine and defective single layer graphene (SLG). We considered 5 different point defects (single-, double-, and tetra- vacancies) observed in the TEM experiments[41, 42]. As for divacancies, three possible configurations, 5-8-5 (**Fig. 1d**), 555-777 **(Fig. 1e**) and 5555-6-7777 **(Fig. 1f**) were considered. We first examined the corresponding total energies of the structures for all possible adsorption sites, and the most stable configurations are shown in **Fig. 1.** Li adsorption on pristine graphene is energetically not favorable with respect to bulk Li phase, as evidenced by positive formation energy, in agreement with the previous reports [39, 43]. In contrast, the presence of undercoordinated atoms in the graphene with defects leads to a negative formation energy of -1.02, -0.51, -0.44 and -0.7 eV for single vacancy and divacancy in the 5-8-5, 5555-6-7777 and 555-777 configurations, respectively. In the lowest energy configurations, Li is located above the center of the octagon ring in the 5-8-5, above the heptagon ring in the 555-777 and on top of the pentagon ring in the 5555-6-7777 defect. In case of tetra vacancies, we

found that Li atom is adsorbed on the hollow site of the octagonal ring with a formation energy of -0.9 eV (**Fig. 1c**). These results suggest that Li atoms are more likely to absorb on vacancies with unsaturated bonds, or defects containing large (8-, 9-membered) non-hexagonal rings.

In order to further analyze the interaction between graphene and Li atoms, the charge density difference plot (**Fig. 1g** and **Fig. S1**) and Bader charge have been obtained (**Table S1**). It can be seen that the electron density around Li is depleted upon adsorption on graphene, but a large fraction of charge density is still localized close to the Li atoms suggesting covalent bonding between Li and C atoms. We note that charge transfer is more pronounced in the case of graphene with tetra vacancy in comparison with pristine graphene, but the bonding trend cannot be explained by charge transfer alone. In any case, it is evident that it is energetically favorable for Li atoms to be adsorbed on defects rather than on the pristine graphene.

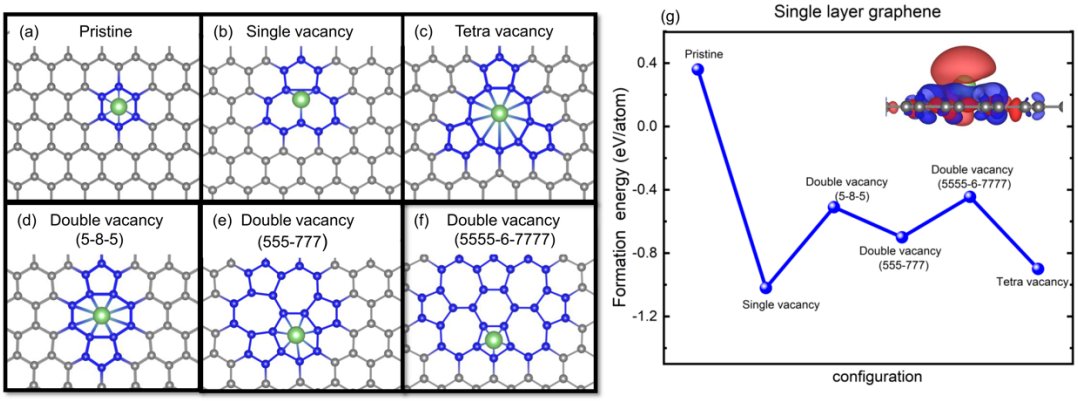

Fig. 1 (a)-(f) Atomic structures of single-layer graphene (SLG) with one lithium atom adsorbed on pristine area, single vacancy, double vacancy (5-8-5), reconstructed double vacancy (555-777), reconstructed double vacancy (5555-6-7777), and tetra vacancy. The C atoms nearest to Li are highlighted. (g) Formation energies of atomic configuration with one Li atom adsorbed on pristine and defective SLG. Charge density difference for one Li atom adsorbed on the tetra vacancy is shown. Blue and red regions represent charge accumulation and charge depletion, respectively.

We further studied Li agglomeration on graphene by introducing the second Li atoms to the system at all inequivalent absorbed sites, while the first Li atom was kept in its

most stable configuration. **Fig. 2a-f** depict the lowest energy structures for two Li atoms adsorbed on different vacancies. We found that (1) formation energy increases with the concentration of Li on pristine graphene; (2) the presence of defects on graphene significantly strengthens the bonding between Li and graphene as compared to the pristine system; (3) for larger vacancies, e.g., the tetra vacancy, the Li-graphene interaction is enhanced, and the formation energy of -0.66 eV/Li is found. As Li atoms donate electrons to the delocalized π states of graphene[44], there is no chemical bonding between the Li ions. The charge density difference plots (**Fig. 2g** and **Fig. S1**) demonstrate that electron density is mostly depleted in the area between two Li ions and graphene surface, especially in tetra vacancy, which reflects charge transfer into bonds with graphene.

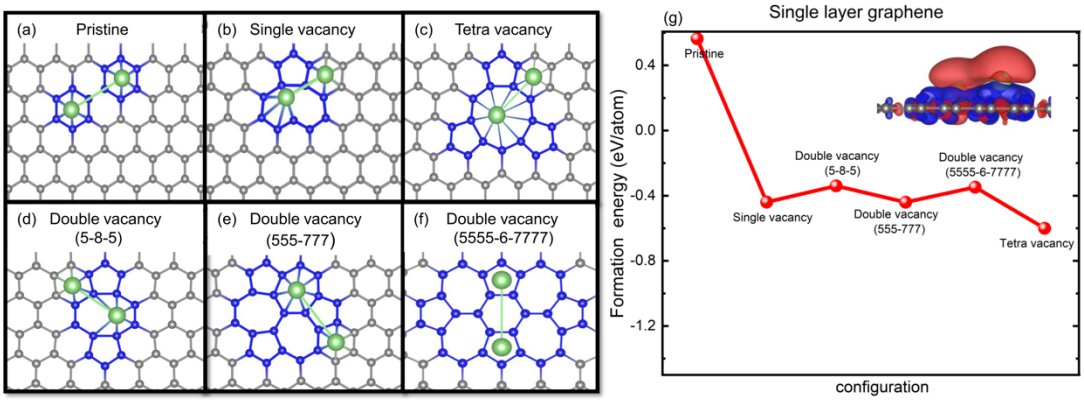

Fig. 2 (a)-(f) Atomic structures of single-layer graphene (SLG) with two lithium atoms adsorbed on pristine area, single vacancy, double vacancy (5-8-5), reconstructed double vacancy (555-777), reconstructed double vacancy (5555-6-7777), and tetra vacancy. (g) Formation energies of atomic configuration with two Li atoms adsorbed on pristine and defective SLG. Charge density difference for two Li atoms adsorbed on the tetra vacancy is shown. Blue and red regions represent charge accumulation and charge depletion, respectively.

3.1.2. Interaction of Li atoms with bilayer graphene

We further studied Li intercalation in the interlayer spacing of bilayer graphene. Upon Li intercalation, the interlayer vdW interaction in the bilayer graphene will be perturbed due to the hybridization between Li ions and carbon atoms[45]. The lowest energy configurations of Li atoms intercalated between AA- and AB-stacked bilayer graphene with various types of defects are presented in **Fig. 3a-f** and **Fig. S3**. The adsorption of Li on pristine graphene, single vacancy, double (5-8-5), (555-777), and (5555-6-7777) vacancy, and tetra vacancy corresponds to the formation energy of -0.37, -1.34, -0.78, -0.92, -0.79 and -1.04 eV/Li, respectively. The formation energies for those defect-free and defective systems with Li intercalating within BLG are lower than those for Li adsorbing SLG (**Fig. 1**) due to the interaction with the other graphene layer. Therefore, Li energetically prefers to intercalate between the interlayer spacing rather than absorb on graphene surface. When compared to the data for AB-stacked graphene (**Fig. S5, Fig. S6**), our results indicate that Li is more inclined to intercalate within AA-stacked BLG than AB-stacked BLG, which is consistent with previous reports [46]. Similar to SLG, charge density difference for Li atoms adsorbed on defect-free and defective BLG exhibit charge accumulation and depletion zones at BLG and Li atoms, respectively (**Fig. 3g** and **Fig. S2**).

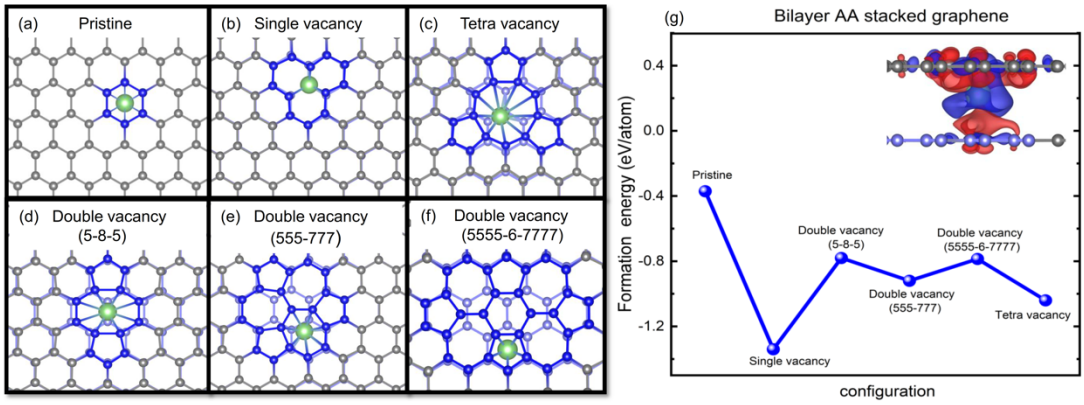

Fig. 3 (a)-(f) Atomic structures of bilayer graphene (BLG) with one lithium atom adsorbed on pristine area, single vacancy, double vacancy (5-8-5), reconstructed double vacancy (555-777), reconstructed double vacancy (5555-6-7777), and tetra vacancy. (g) Formation energies of atomic configurations of one Li atom adsorbed on pristine

and defective BLG. Charge density difference for one Li atom adsorbed on the tetra vacancy is shown. Blue and red regions represent charge accumulation and charge depletion, respectively.

Formation energies of atomic configurations involving two Li atoms adsorbed on AA-stacked BLG were to evaluated to assess the tendency of Li atoms towards clustering between the layers. The most stable configurations of defect-free, single vacancy, double vacancy (5-8-5), double vacancy (555-777), double vacancy (5555-6-7777), and tetra vacancy are depicted in **Fig. 4a-f,** with the corresponding formation energies of -0.27, -0.81, -0.71, -0.85, -0.76 and -0.97 eV/atom, respectively. The strong interactions between Li and tetra vacancy can be associated with the substantial charge transfer, as evident from **Fig. 4-f.** Similar to the behavior of a single Li atom, there is a large charge depletion region around Li atoms for all types of the considered defects, which indicates strong charge transfer between Li atoms and graphene layers **(Fig. S2)**.

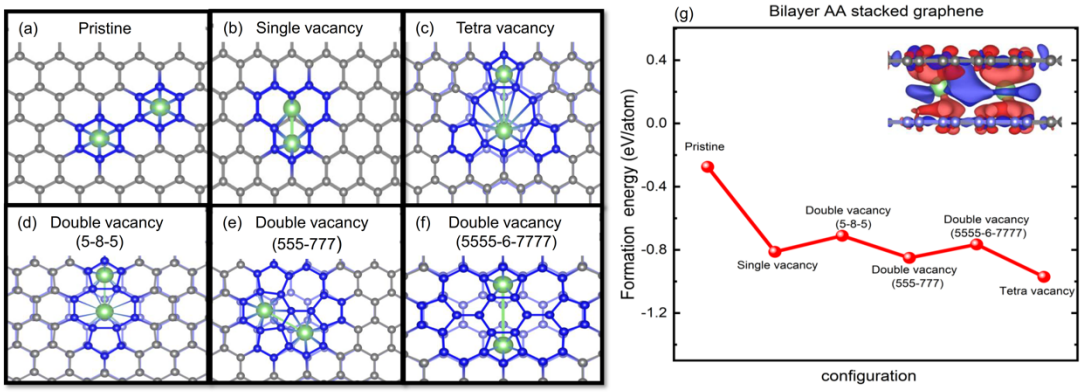

Fig. 4 (a)-(f) Atomic structures of bilayer graphene (BLG) with two lithium atoms adsorbed on pristine area, single vacancy, double vacancy (5-8-5), reconstructed double vacancy (555-777), reconstructed double vacancy (5555-6-7777), and tetra vacancy. (g) Formation energies of atomic configurations of two Li atoms adsorbed on pristine and defective BLG. Charge density difference for two Li atoms adsorbed on the tetra vacancy is shown. Blue and red regions represent charge accumulation and charge depletion, respectively.

3.1.3. Comparison of the energetics of Li interaction into single and bilayer graphene

Aiming at understanding the role of structural defects in agglomeration of Li atoms, we compared the stability of the atomic configuration involving Li atoms absorbed at defect sites of graphene with those separated over defect and pristine areas (**Fig. 5a**). The increase in Li coverage results in less favorable Li adsorption on pristine graphene due to increasing the Coulomb repulsion between the positively charged Li ions. In contrast, the difference in formation energy for graphene with defects shows negative value indicating that increasing Li atom concentration causes Li adsorption to be energetically favorable on defects (with Li atoms already present) rather than in the pristine area (**Fig. 5b**)**.** This is also evident from shorter Li-Li distances on defective graphene (3.08-3.89 Å) in comparison to the corresponding value for the pristine graphene (4.33 Å). The formation energy difference decreases with the size of the defect following the sequence of ΔE_f (tetra vacancy) $<\Delta E_f(5555-6-7777) <$ $\Delta E_f(555-777) < \Delta E_f(5-8-5) < \Delta E_f$ (single vacancy) $< \Delta E_f$ (pristine). These results suggest that Li atoms tend to aggregate on defects (especially larger defects) in graphene. Similar to SLG, ΔE_f becomes more positive with inserting more Li atoms into pristine bi-layer graphene, while the energy penalty decreases in the presence of defects suggesting that Li nucleation is likely to be at the defect sites (**Fig. 5c**). As the number of adsorbed Li atoms increases, the dangling bonds at the defective graphene are gradually saturated and hence the formation energies approach the values of pristine graphene for an infinite number of Li atoms **(Fig. S7)**.

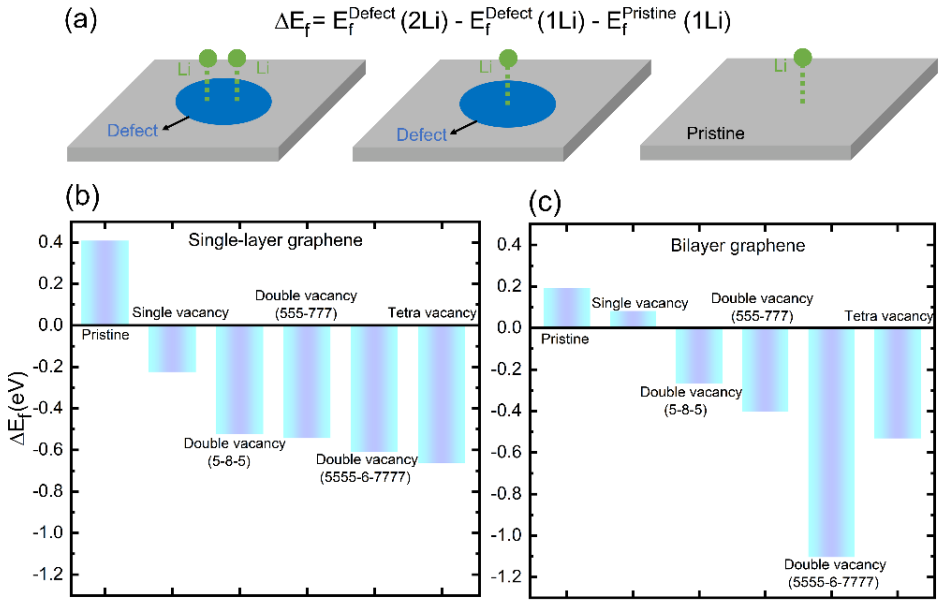

Fig. 5 (a) Schematic representation of Li atoms adsorbed on graphene with and without defects. (b) The difference in the formation energy of Li-defect configurations between single-layer and (c) bilayer graphene with various types of defects.

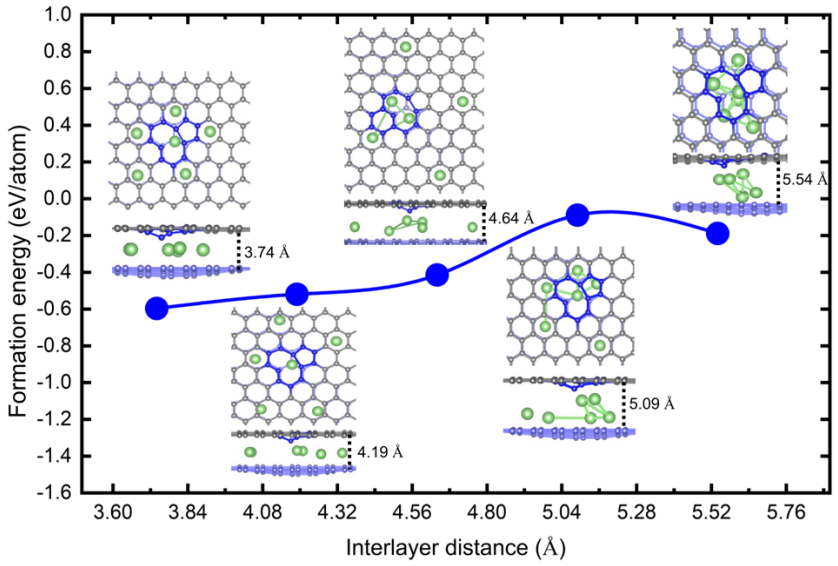

Fig. 6 Structural evolution of Li clusters for different interlayer distances of bilayer graphene. The defective areas in graphene are highlighted.

The creation of Li dendrites on graphene layer has already been experimentally and theoretically investigated[26, 47, 48]. However, the nucleation of Li clusters between bilayer graphene has not yet been addressed. Here, we studied the energetics of small

Li clusters (6 atoms) intercalated between two graphene sheets with different interlayer spacing (**Fig. 6**). We note that the spacing may be affected by other Li clusters already formed or by impurities or hydrocarbon molecules, which are inevitably present in the experiments. The formation energy initially goes up with interlayer distance ($d_{\text{interlayer}}$) up to a maximum (less favorable) value and then decreases for $d_{\text{interlayer}} > 5.1$ Å. As evident from the figure, an energy barrier of about 0.4 eV for the clustering of Li atoms exist. From the structural point of view, increasing the distance leads to a distortion of the planar Li cluster where the middle Li atom next to the defect moves upwards. By further increasing the spacing, more Li atoms agglomerate around the defect, and formation of Li clusters is energetically preferred over plane configuration. It should be noted that the concentration of Li ions has a significant impact on Li nucleation barrier[26]. In small Li clusters (consisting of a few atoms), there are no low-energy facets corresponding to well-defined crystal surfaces which normally exist in large metal particles. As a result, even a slight change in cluster configuration leads to a considerable energy variation and consequently different nucleation barriers. In larger clusters, however, the surface energy plays a major role and the energetics of cluster geometries do not significantly change by variation of Li atoms. Therefore, one can expect that the transition barrier is further reduced for larger Li clusters during excessive Li intercalation into the interlayer space. To this end, the presence of defects combined with weak interlayer interactions can facilitate the agglomeration of lithium crystals between bilayer graphene.

We note that these results are not strict, as there are many possible atomic configurations for Li clusters. Our main goal here is to provide a qualitative discussion of how multi-layer structures can appear. As mentioned above, either for pristine or defective graphene, the commensurate $(\sqrt{3}\times\sqrt{3})$R30° configuration has the lowest formation energy. We have tried different initial configurations for each interlayer distances starting from the interatomic Li distances in the FCC lithium structure and the most stable structures were shown in **Fig. 6**. It is possible that the reported geometries do not represent the lowest energy configurations for these clusters; nevertheless, given the inherent polymorphism of few-atom metal clusters, their

energies are quite close to them. We also note that an increase in the interlayer separation between graphene sheets (due to thermal fluctuations or other reasons) should facilitate the formation of multi-layer Li structures.

3.2 Atomic structure of the interface between q-2D Li crystals and graphene

3.2.1 Atomic structure of the interface between (111) FCC Li crystal and pristine graphene

In light of the recent studies[24] where q-2D Li crystals were observed in BLG, it is also important to understand the atomic structure of the interface between Li crystals with pristine and defective graphene. The calculated interlayer binding energy of graphene on (111) facet of Li is ~37 meV/Å^2, somewhat lower than in pure vdW system[49], pointing to a small contribution of ionic bonding due to charge transfer, as also discussed previously[35]. **Fig. 7** shows the atomic structure of the graphene-Li interface where atoms are colored according to their *z*-coordinates (different scales for Li and C atoms). The graphene layer exhibits slight bucking due to the different match and thus different interaction between the atoms in different areas of the moiré pattern at the interface. Similar development of the moiré pattern has been reported for graphene on many FCC metal substrates including Rh (111), Ir(111) and Ru(0001) [50-52]. Three regions in the moiré pattern can be identified depending on the positions of carbon atoms with respect to the Li atoms underneath, **Fig. 8a**: (1) TOP region: the center of the C hexagon located on top of a Li atom. (2) FCC region: a Li atom from the third Li layer is located below the middle of the C hexagon. (3) HCP region: center of C hexagon is above a Li atom in the second layer. In the TOP-region, three C atoms of one graphene hexagon are found in a fcc site (TOP-fcc) and three in a hcp site (TOP-hcp). Similarly, other positions in FCC and HCP regions can be specified.

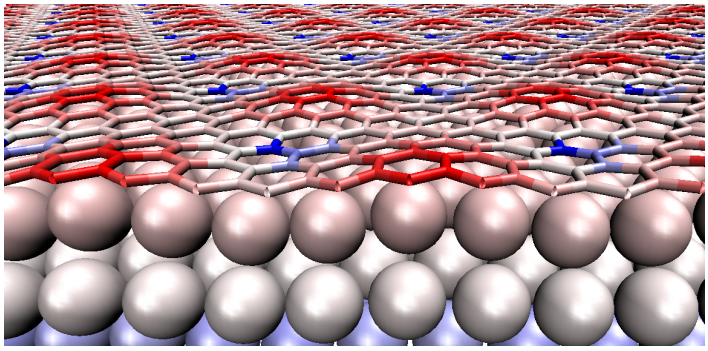

Fig. 7 Atomic structure of the interface between Li FCC crystal and graphene sheet. Li atoms are shown as large balls. Atoms are colored according to their z coordinate, red (high) to blue (low). The development of the moiré pattern is evident.

3.2.2 Formation energy of various defects at the graphene/Li (111) interface

Having studied the interface between the pristine graphene and (111) surface of FCC Li, we moved on to the defective graphene. In total, six representative configurations of graphene with single vacancies facing Li (111) surface were considered. A significant variation in the formation energy was found for different positions of defects in the supercell, as evident from **Fig. 8b-g**. Single vacancies prefer to be exactly on top of a Li atom. The optimum positions of single vacancies in three different regions lead to lower formation energy in FCC and HCP regions, as compared to the TOP region (**Fig. 8b-g**). This can be attributed to energy release due to stronger interaction between carbon atoms with dangling bonds and Li atoms underneath (**Fig. 8)**. The top site in the FCC region **(Fig. 8b)**, is the most stable configuration in all considered vacancy sites. The formation energy of C vacancy in the TOP regions is higher, as there is no match between the underlying Li and the C atoms with dangling bonds. The formation energies of vacancies, with the values about 5 eV, are notably lower than those in the free-standing graphene (~7.4 eV) [41]. In addition to single vacancies, double and tetra vacancies at the graphene-Li interface were considered **(Fig. S8)**. The formation energy of double vacancy (555-777) was found to be lower than single vacancies indicating stronger interaction between Li surface with undercoordinated C atoms in larger defects. Similar trends in vacancy formation energies have previously been reported for graphene on other FCC metals, e.g., iridium[53]. The binding between Li with vacancy

defects in graphene was further studied by analyzing the electronic density of states (DOS) close to the Fermi level (**Fig. S9**). The presence of the defects increases the electron density above the Fermi level (energy interval from 0 to 0.1 eV). This corresponds to the hybridization between unfilled s valence orbital of metal atoms[54] and defect-associated states in graphene. As for larger defects (with more delocalized states) and more metal atoms, the C-Li hybridization may be extended in the energy window as shown before in Ref 54.

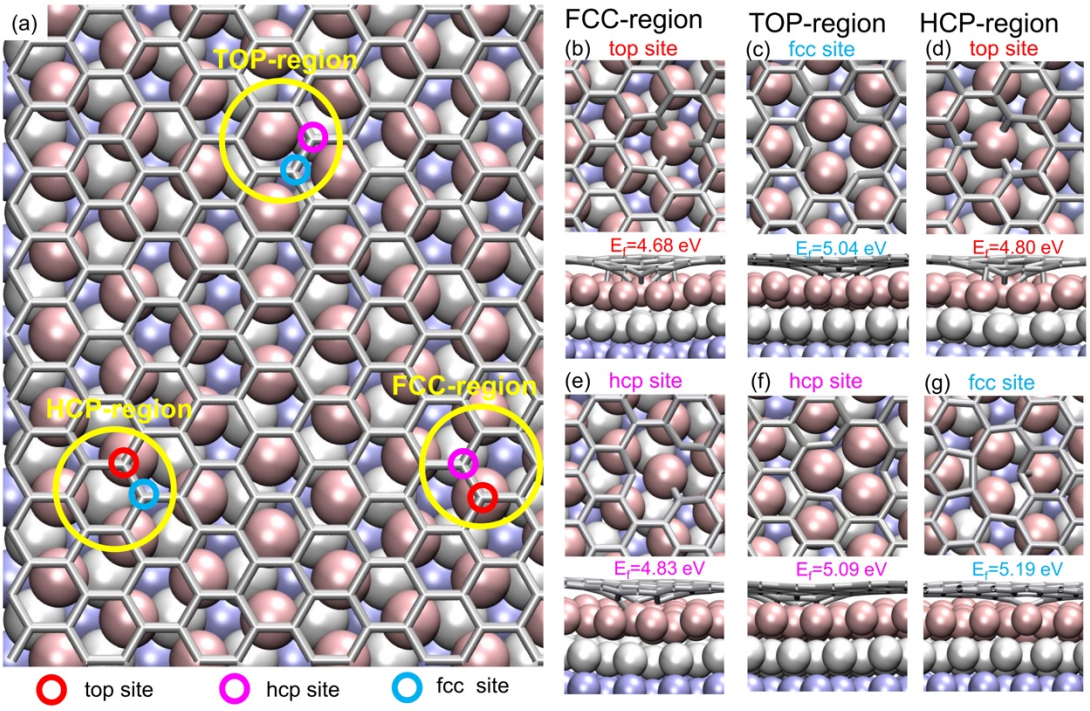

Fig. 8 Atomic structures of the interface graphene and (111) surface of FCC Li crystals. (a) Defect-free graphene/Li (111) interface. Regions of high symmetry (HCP, FCC, TOP region) are depicted by large yellow circles. The sites of selected individual carbon atoms are indicated by colored small circles. Li atoms are colored according to their elevation. (b−g) Top and side views of a single vacancies in different areas of the moiré pattern. Formation energies of vacancies are also presented.

As the drop in vacancy formation energies is associated with the strong interaction between vacancies and Li atoms in the crystal, which gives rise to lower vacancy formation energies (about 2.5 eV lower than for the free-standing graphene), one can conclude that q-2D Li crystallites must be strongly bound to graphene vacancies. One

can arrive at the same conclusion if the binding energy of the crystallite to graphene with and without vacancy is calculated: with vacancy the binding energy decreases by about 1 eV. Thus, a Li crystallite, if nucleated, should remain attached to the defect in graphene.

3.3. Interaction of graphene edge with Li cluster

It is known that vacancies in graphene can agglomerate into vacancy clusters (or holes), as the number of dangling bonds per missing atom is reduced. We investigated the interaction of Li atoms with large vacancy clusters in graphene using a simple ribbon model assuming that the atomic structure of the edge is the same as in the hole (zigzag edge, which has lower formation energy than armchair edge[55]. As demonstrated in the previous experimental studies, the presence of graphene edges changes the crystallinity and image contrast of Li crystals intercalated between bilayer graphene[18]. Computations have shown that the interactions between Li atoms and graphene nanoribbons (GNRs) depend on the edge geometry suggesting that the adsorption of Li atoms on zigzag GNRs is more favorable than on armchair GNRs due to electronic states localized at the zigzag edges[56]. Accordingly, in the present study we focused on Li adsorption on zigzag GNRs. The number of Li atoms adsorbed on the edge varied from 1 to 7. In contrast to vacancies, which are too small to accommodate Li atoms, Li adsorption takes place preferentially in the graphene plane with the exact position of Li atom being between two carbon atoms at the zigzag edge (**Fig. 9**). The formation energy of a configuration with single Li atom on the edge is -1.80 eV, which is lower than for pristine graphene and vacancies. The formation energy per atom increases with the number of Li atoms, implying the repulsive interaction between Li atoms on the edge. To understand how Li atoms agglomerate at the edges, we compared the energetics of a 2D Li cluster with the energy of the same number of adsorbed at graphene edge and forming a chain (**Fig. 9-e**). The formation energy of the Li chain (-1.48 eV/atom) is lower than that of the cluster (**Fig. 9-f**, -0.51 eV/atom) due to the stronger interaction of Li atoms with carbon atoms at the edge in comparison with the binding energies between Li atoms in the cluster. The large energy gain through the Li

adsorption on graphene edge is in agreement with the experimental observations[57-59] that limited spacing between graphene sheets prevents the growth of compact 3D Li structures. Our results indicate that the edges of large holes in graphene can easily pick up Li atoms, but once the edges are fully lithiated, adsorption on vacancies in graphene should become preferable over cluster growth. For the same number of Li atoms, the formation energy is lowest when Li is adsorbed at the edge of graphene and form the chain, which is followed by when Li is adsorbed by small vacancies, and finally when Li atoms form a cluster (see **Table S2**).

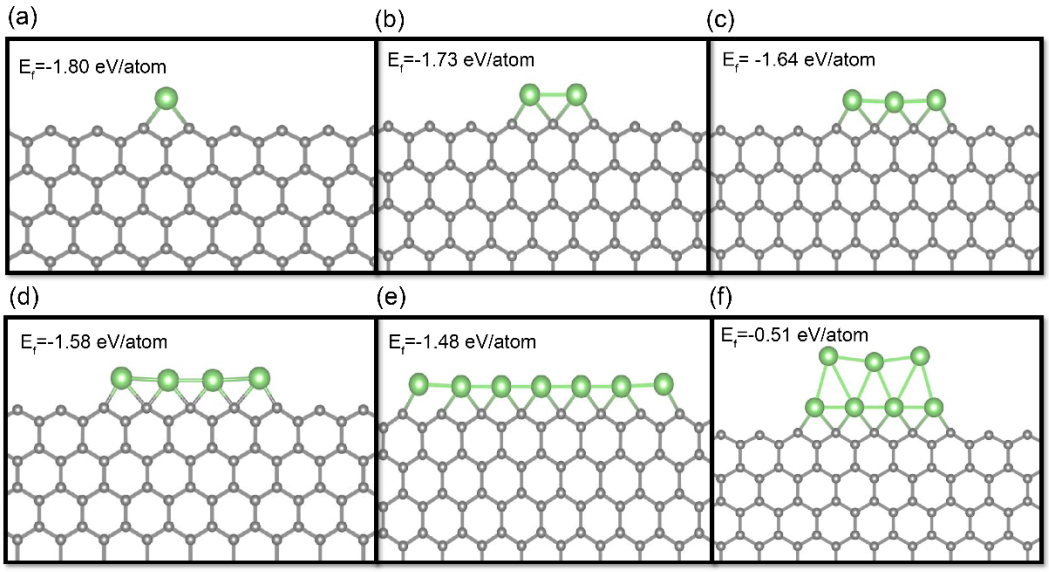

Fig. 9 Schematic representations for Li atoms (n_{Li}=1, 2, 3, 4, 7) adsorbed on graphene edge. The green and gray colored balls represent Li and carbon atoms, respectively.

3.4. Impurities in Li crystals intercalated into bilayer graphene

TEM in-situ experiments[18] of lithiation and delithiation of BLG indicated that impurity atoms are present in the system strongly affecting the delithiation process so that not all Li atoms are removed and amorphous Li structures (most likely oxides) remain inside BLG. The positions of the impurity atoms were found to match Li atom columns, but it was not clear, though, if they are at the interface between graphene and Li, or inside the crystal. Based on the stronger contrast and electron energy-loss spectroscopy data, it was concluded that these are likely oxygen atoms, although the presence of other atomic species which can strongly interact with Li (nitrogen, fluorene,

sulfur) could not fully be excluded. These observations may shed light on the reduction of the Li battery capacity after cycles, so that it is important to understand the behavior of impurities in Li crystals.

We simulated O, N, F, and S impurities in the BLG-Li system (**Fig. 10**), the latter being represented by three layers of Li atoms. The impurity atom was initially placed between graphene and Li crystal and the structure was fully optimized. We found all the impurity atoms go without any potential barrier into the sub-surface area of the crystal, and take the octahedral interstitial position there, so that they are indeed in Li atom columns. Similar behavior has been reported for C atoms on the (111) copper surface[60]. The position of N impurity is shown in **Fig. 10a,c**. It is essentially the same for all the elements we considered, although it was slightly distorted for S impurity.

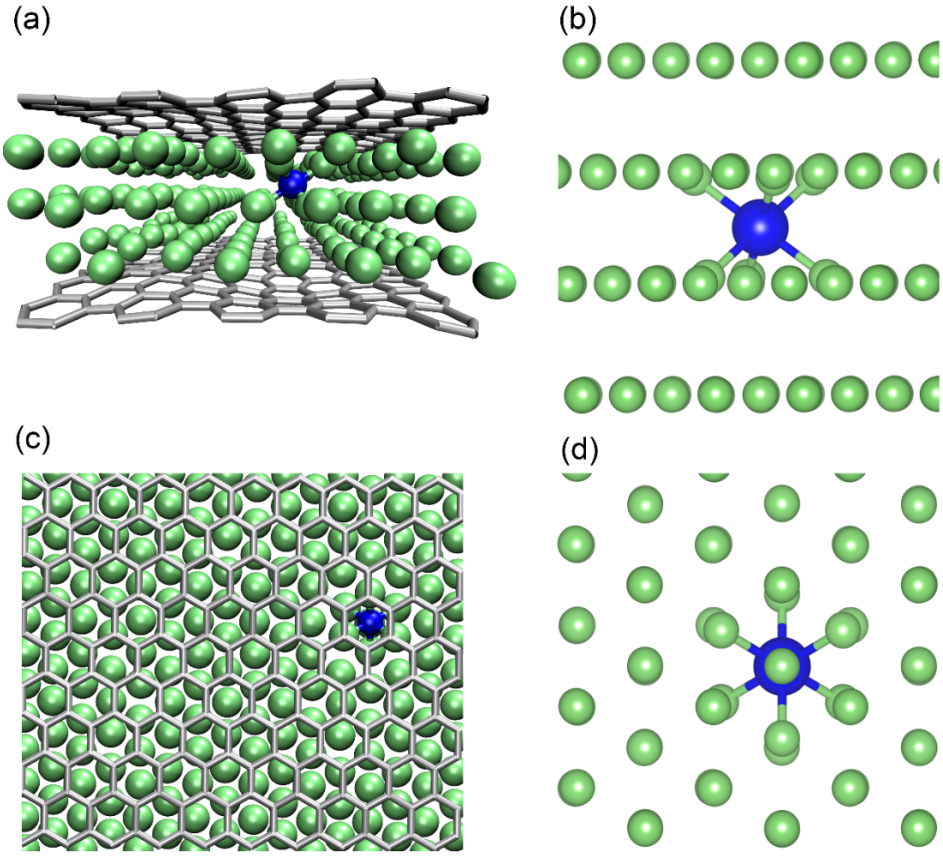

Fig. 10 Nitrogen atom in the octahedral interstitial position in the FCC q-2D Li crystallite consisting of three Li layers between graphene sheets, side (a) and top (c) views. Octahedral interstitials (N, O, F, S) in the bulk Li crystal, side (b) and top (d) views.

As interstitials in FCC metals can also take tetrahedral and substitutional positions[61], which could also coincide with the atom columns, we further assessed the energetics of tetra/octa interstitials and impurities by evaluating the energy released when an isolated impurity atom is inserted into the crystal as intestinal:

$$E_f^{inter} = E_{slab+impurity} - [E_{slab} + E_{impurity}] \quad (4)$$

or substitutional impurity atom:

$$E_f^{subst} = E_{slab+impurty} + \mu_{Li} - [E_{slab} + E_{impurity}] \quad (5)$$

Here E_{slab} and $E_{slab+impurty}$ represent the total energy of Li slab without and with impurity, respectively. $E_{impurity}$ is the energy of an isolated impurity atom and μ_{Li} indicates the chemical potential of Li in the bulk elemental (FCC) phase.

We could not stabilize the tetrahedral interstitials in the tri-layer system as they converted to the octa configurations. Thus, keeping in mind that Li crystals in BLG observed in the experiments consisted up to 9 layers, we also calculated the formation energies of the defects for bulk crystals modelled as a slab composed from 576 Li atoms. The results of calculations are presented in **Table 1**. It is evident that the interstitials in the octahedral configurations are always energetically favorable, and that the interaction of the impurity atoms with Li is very strong, so that stable neutral impurity-Li complexes can be formed and remain between graphene sheets upon de-lithiation. The same conclusion can be drawn from the comparison of the energetics of Li atoms when in the infinite Li crystal and in Li_xO (x=1, 2, 3, 4) molecules, **Table S3**. It is evident that it is energetically more favorable for a Li atom to form a Li_xO molecule than to be in the crystal, which should affect the de-lithiation process.

Table 1. Formation energies (in eV) of interstitial atoms in the bulk FCC Li crystal and tri-layer Li between graphene sheets. *For S, the octahedral configuration in the tri-layer Li crystal between graphene sheets was slightly distorted.

	N	O	F	S
octa	-6.47	-8.69	-6.73	-6.17
tetra	-5.13	-7.63	-6.60	-5.50

subs	-5.51	-8.18	-5.36	-5.94
3L+GR, octa	-6.49	-8.79	-6.85	-6.70*

4. Conclusions

We have investigated the interaction of Li atoms with pristine and defective single layer and bilayer graphene using first-principles calculations and showed that they prefer to adsorb on point defects in graphene and graphene edges. We also systematically studied the atomic structure of the interface between the q-2D FCC Li crystals with vacancy-type defects in graphene and showed that not only isolated atoms, but also q-2D Li crystals encapsulated between graphene sheets are strongly bound to the defects. These findings explain the experimental observations of the predominant nucleation and growth of q-2D FCC Li crystals at defects in BLG. We further demonstrated that a moiré pattern is present at the graphene/Li interface, and the formation energy of vacancies in graphene depends on their location in the moiré pattern. The moiré pattern can potentially be revealed in scanning tunneling probe microscopy experiments on lithiated BLG on substrates. We also studied the behavior of impurity atoms most likely to be found in the encapsulated Li crystals, such as O, N, S and F. Our calculations indicate that all impurity atoms take octahedral interstitial positions in Li crystals, but not between graphene and Li. They strongly interact with atoms in Li crystals, thus impeding the de-lithiation process. Although our theoretical work is primarily focused on the fundamental aspects of the behavior of Li inside bilayer graphene, our findings can help rationalize the results of in-situ TEM experiments and shed light on the role of impurities in the degradation of anode materials during Li-ion battery operation.

Declaration of competing interest

The authors declare that they have no known competing financial interests or personal relationships that could have appeared to influence the work reported in this paper.

Acknowledgements

We thank Prof. Ute Kaiser and Dr. Yueliang Li for sharing the unpublished TEM data with us. The authors would like to acknowledge University of Science and Technology of China (USTC) and China Scholarship Council (CSC) for supporting this research project. We further thank the German Research Foundation (DFG) through projects KR 4866/8-1 and the collaborative research center "Chemistry of Synthetic 2D Materials" CRC-1415-417590517. Generous CPU time grants from the Technical University of Dresden computing cluster (TAURUS) and Gauss Centre for Supercomputing e.V. (www.gauss-centre.eu), Supercomputer HAWK at Höchstleistungsrechenzentrum Stuttgart (www.hlrs.de), are greatly appreciated.

Data availability

Details of the calculations presented in the manuscript and supplementary information should be sufficient to reproduce the results. Input files can also be provided upon request.

References

[1] M.S. Whittingham, Lithium batteries and cathode materials, Chem. Rev. , 104 (2004) 4271−4301. https://doi.org/10.1021/cr020731c.

[2] J. Muldoon, C.B. Bucur, T. Gregory, Quest for nonaqueous multivalent secondary batteries: Magnesium and beyond, Chem. Rev., 114 (2014) 11683-11720. https://doi.org/10.1021/cr500049y.

[3] L. Shi, T. Zhao, Recent advances in inorganic 2D materials and their applications in Lithium and Sodium batteries, J. Mater. Chem. A, 5 (2017) 3735-3758. https://doi.org/10.1039/C6TA09831B.

[4] R. Rojaee, R. Shahbazian-Yassar, Two-dimensional materials to address the Lithium battery challenges, ACS Nano, 14 (2020) 2628-2658. https://doi.org/10.1021/acsnano.9b08396.

[5] J. Xu, Y. Dou, Z. Wei, J. Ma, Y. Deng, Y. Li, H. Liu, S. Dou, Recent progress in graphite intercalation compounds for rechargeable metal (Li, Na, K, Al)-ion batteries, Adv. Sci. , 4 (2017) 1700146. https://doi.org/10.1002/advs.201700146.

[6] J. Janek, W.G. Zeier, A solid future for battery development, Nat. Energy, 1 (2016) 1-4. https://doi.org/10.1038/nenergy.2016.141.

[7] F.J. Sonia, M.K. Jangid, B. Ananthoju, M. Aslam, P. Johari, A. Mukhopadhyay, Understanding the Li-storage in few layers graphene with respect to bulk graphite: experimental, analytical and computational study, J. Mater. Chem. A, 5 (2017) 8662-8679. https://doi.org/10.1039/C7TA01978E.

[8] K. Ji, J. Han, A. Hirata, T. Fujita, Y. Shen, S. Ning, P. Liu, H. Kashani, Y. Tian, Y. Ito, J.I. Fujita, Y. Oyama, Lithium intercalation into bilayer graphene, Nat. Commun. , 10 (2019) 275.

https://doi.org/10.1038/s41467-018-07942-z.
[9] W. Bao, J. Wan, X. Han, X. Cai, H. Zhu, D. Kim, D. Ma, Y. Xu, J.N. Munday, H.D. Drew, M.S. Fuhrer, L. Hu, Approaching the limits of transparency and conductivity in graphitic materials through Lithium intercalation, Nat. Commun., 5 (2014) 4224. https://doi.org/10.1038/ncomms5224.
[10] D.K. Bediako, M. Rezaee, H. Yoo, D.T. Larson, S.Y.F. Zhao, T. Taniguchi, K. Watanabe, T.L. Brower-Thomas, E. Kaxiras, P. Kim, Heterointerface effects in the electrointercalation of van der Waals heterostructures, Nature, 558 (2018) 425-429. https://doi.org/10.1038/s41586-018-0205-0.
[11] S. Ichinokura, K. Sugawara, A. Takayama, T. Takahashi, S. Hasegawa, Superconducting Calcium-intercalated bilayer graphene, ACS Nano, 10 (2016) 2761-2765. https://doi.org/10.1021/acsnano.5b07848.
[12] A.P. Durajski, K.M. Skoczylas, R. Szczesniak, Superconductivity in bilayer Graphene intercalated with Alkali and Alkaline earth metals, Phys. Chem. Chem. Phys., 21 (2019) 5925-5931. https://doi.org/10.1039/C9CP00176J.
[13] M. Kuhne, F. Paolucci, J. Popovic, P.M. Ostrovsky, J. Maier, J.H. Smet, Ultrafast lithium diffusion in bilayer graphene, Nat. Nanotechnol., 12 (2017) 895-900. https://doi.org/10.1038/nnano.2017.108.
[14] K. Chang, W. Chen, In situ synthesis of MoS_2/graphene nanosheet composites with extraordinarily high electrochemical performance for Lithium ion batteries, Chem. Commun., 47 (2011) 4252-4254. https://doi.org/10.1039/C1CC10631G.
[15] K. Chang, W. Chen, L-cysteine-assisted synthesis of layered MoS_2/graphene composites with excellent electrochemical performances for lithium ion batteries, ACS Nano, 5 (2011) 4720–4728. https://doi.org/10.1021/nn200659w.
[16] R.I. Pushparaj, D. Cakir, X. Zhang, S. Xu, M. Mann, X. Hou, Coal-derived graphene/MoS_2 heterostructure electrodes for Li-ion batteries: experiment and simulation study, ACS Appl. Mater. Interfaces, 13 (2021) 59950-59961. https://doi.org/10.1021/acsami.1c18993.
[17] I.V. Chepkasov, J.H. Smet, A.V. Krasheninnikov, Single- and Multilayers of Alkali metal atoms inside graphene/MoS_2 heterostructures: A systematic first-principles study, J. Phys. Chem. C, 126 (2022) 15558-15564. https://doi.org/10.1021/acs.jpcc.2c03749.
[18] M. Kuhne, F. Borrnert, S. Fecher, M. Ghorbani-Asl, J. Biskupek, D. Samuelis, A.V. Krasheninnikov, U. Kaiser, J.H. Smet, Reversible superdense ordering of Lithium between two graphene sheets, Nature, 564 (2018) 234-239. https://doi.org/10.1038/s41586-018-0754-2.
[19] Y.C. Lin, A. Motoyama, S. Kretschmer, S. Ghaderzadeh, M. Ghorbani-Asl, Y. Araki, A.V. Krasheninnikov, H. Ago, K. Suenaga, Polymorphic phases of metal chlorides in the onfined 2D space of bilayer graphene, Adv. Mater., 33 (2021) 2105898. https://doi.org/10.1002/adma.202105898.
[20] K. Mustonen, C. Hofer, P. Kotrusz, A. Markevich, M. Hulman, C. Mangler, T. Susi, T.J. Pennycook, K. Hricovini, C. Richter, J.C. Meyer, J. Kotakoski, V. Skakalova, Toward exotic layered materials: 2D cuprous iodide, Adv. Mater., 34 (2022) 2106922. https://doi.org/10.1002/adma.202106922.
[21] T. Lehnert, S. Kretschmer, F. Brauer, A.V. Krasheninnikov, U. Kaiser, Quasi-two-dimensional NaCl crystals encapsulated between graphene sheets and their decomposition under an electron beam, Nanoscale, 13 (2021) 19626-19633. https://doi.org/10.1039/D1NR04792B.
[22] H. Kinoshita, I. Jeon, M. Maruyama, K. Kawahara, Y. Terao, D. Ding, R. Matsumoto, Y. Matsuo, S. Okada, H. Ago, Highly conductive and transparent large-area bilayer graphene realized by $MoCl_5$ intercalation, Adv. Mater., 29 (2017) 1702141. https://doi.org/10.1002/adma.201702141.
[23] C. Zhang, K.L. Firestein, J.F.S. Fernando, D. Siriwardena, J.E. von Treifeldt, D. Golberg, Recent progress of in situ transmission electron microscopy for energy materials, Adv. Mater., 32 (2020)

1904094. https://doi.org/10.1002/adma.201904094.
[24] Y. Li, F. Börrnert, S. Fecher, Z. Li, J. Biskupek, S. Yang, M. Kühne, D. Bresser, J.H. Smet, U. Kaiser, to be published.
[25] X. Fan, W.T. Zheng, J.L. Kuo, D.J. Singh, Adsorption of single Li and the formation of small Li clusters on graphene for the anode of Lithium-ion batteries, ACS Appl. Mater. Interfaces, 5 (2013) 7793-7797. https://doi.org/10.1021/am401548c.
[26] M. Liu, A. Kutana, Y. Liu, B.I. Yakobson, First-principles studies of Li nucleation on graphene, J. Phys. Chem. Lett., 5 (2014) 1225-1229. https://doi.org/10.1021/jz500199d.
[27] G.D. Lee, C.Z. Wang, E. Yoon, N.M. Hwang, D.Y. Kim, K.M. Ho, Diffusion, coalescence, and reconstruction of vacancy defects in graphene layers, Phys. Rev. Lett., 95 (2005) 205501. https://doi.org/10.1103/PhysRevLett.95.205501.
[28] J. Kotakoski, A.V. Krasheninnikov, U. Kaiser, J.C. Meyer, From point efdects in graphene to two-idmensional amorphous carbon, Phys. Rev. Lett., 106 (2011) 105505. https://doi.org/10.1103/PhysRevLett.106.105505.
[29] J.F. G Kresse, Efficient iterative schemes for ab initio total-energy calculations using a plane-wave basis set, Phys. Rev. B, 54 (1966) 11169. https://doi.org/10.1103/PhysRevB.54.11169.
[30] G. Kresse, and Daniel Joubert., From ultrasoft pseudopotentials to the projector augmented-wave method, Phys. Rev. B, 59 (1999) 1758. https://doi.org/10.1103/PhysRevB.59.1758.
[31] W. Kohn, L.J. Sham, Self-consistent equations including exchange and correlation effects, Phys. Rev., 140 (1965) 1133-1138. https://doi.org/10.1103/PhysRev.140.A1133.
[32] J.P. Perdew, K. Burke, M. Ernzerhof, Generalized Gradient Approximation made simple, Phys. Rev. Lett., 77 (1996) 3865. https://doi.org/10.1103/PhysRevLett.77.3865.
[33] C.M.-L.a.J.A. S. Grimme, Noncovalent interactions between rgaphene sheets and in multishell (hyper) fullerenes, J. Phys. Chem. C, 111 (2007) 11199-11207. https://doi.org/10.1021/jp0720791.
[34] J.A.a.S. Grimme, Structures and interaction energies of stacked graphene–nucleobase complexes, Phys. Chem. Chem. Phys., 10 (2008) 2722–2729. https://doi.org/10.1039/B718788B.
[35] I.V. Chepkasov, M. Ghorbani-Asl, Z.I. Popov, J.H. Smet, A.V. Krasheninnikov, Alkali metals inside bi-layer graphene and MoS_2: insights from first-principles calculations, Nano Energy, 75 (2020) 104927. https://doi.org/10.1016/j.nanoen.2020.104927.
[36] H.J. Monkhorst, J.D. Pack, Special points for Brillouin-Zone integrations, Phys. Rev. B, 13 (1976) 5188. https://doi.org/10.1103/PhysRevB.13.5188.
[37] K. Momma, F. Izumi, VESTA: A three-dimensional visualization system for electronic and structural analysis, J. Appl. Crystallogr., 41 (2008) 653-658. https://doi.org/10.1107/S0021889808012016.
[38] W. Humphrey, A. Dalke, K. Schulten, VMD: Visual Molecular Dynamics, J. Mol. Graphics, 14 (February 1996) 33-38. https://doi.org/10.1016/0263-7855(96)00018-5.
[39] H. Yildirim, A. Kinaci, Z.J. Zhao, M.K. Chan, J.P. Greeley, First-principles analysis of defect-mediated Li adsorption on graphene, ACS Appl. Mater. Interfaces, 6 (2014) 21141-21150. https://doi.org/10.1021/am506008w.
[40] P.V. Medeiros, F. de Brito Mota, A.J. Mascarenhas, C.M. de Castilho, Adsorption of monovalent metal atoms on graphene: A theoretical approach, Nanotechnology, 21 (2010) 115701. https://doi.org/10.1088/0957-4484/21/11/115701.
[41] F. Banhart, J. Kotakoski, A.V. Krasheninnikov, Structural defects in graphene, ACS Nano, 5 (2011) 26-41. https://doi.org/10.1021/nn102598m.
[42] P.T. Araujo, M. Terrones, M.S. Dresselhaus, Defects and impurities in graphene-like materials,

Mater. Today, 15 (2012) 98-109. https://doi.org/10.1016/S1369-7021(12)70045-7.
[43] E. Lee, K.A. Persson, Li absorption and intercalation in single layer graphene and few layer graphene by first principles, Nano. Lett., 12 (2012) 4624-4628. https://doi.org/10.1021/nl3019164.
[44] Y. Liu, Y.M. Wang, B.I. Yakobson, B.C. Wood, Assessing carbon-based anodes for Lithium-ion batteries: a universal description of charge-transfer binding, Phys. Rev. Lett., 113 (2014) 028304. https://doi.org/10.1103/PhysRevLett.113.028304.
[45] K. Persson, Y. Hinuma, Y.S. Meng, A. Van der Ven, G. Ceder, Thermodynamic and kinetic properties of the Li-graphite system from first-principles calculations, Phys. Rev. B, 82 (2010) 125416. https://doi.org/10.1103/PhysRevB.82.125416.
[46] S.N. Shirodkar, E. Kaxiras, Li Intercalation at graphene/hexagonal boron Nitride interfaces, Phys. Rev. B, 93 (2016) 245438. https://doi.org/10.1103/PhysRevB.93.245438.
[47] S.J. Harris, A. Timmons, D.R. Baker, C. Monroe, Direct in situ measurements of Li transport in Li-ion battery negative electrodes, Chem. Phys. Lett., 485 (2010) 265-274. https://doi.org/10.1016/j.cplett.2009.12.033.
[48] M.Z. Mayers, J.W. Kaminski, T.F. Miller, Suppression of dendrite formation via pulse charging in rechargeable Lithium metal batteries, J. Phys. Chem. C, 116 (2012) 26214-26221. https://doi.org/10.1021/jp309321w.
[49] T. Bjorkman, A. Gulans, A.V. Krasheninnikov, R.M. Nieminen, van der Waals bonding in layered compounds from advanced density-functional first-principles calculations, Phys. Rev. Lett., 108 (2012) 235502. https://doi.org/10.1103/PhysRevLett.108.235502.
[50] E.N. Voloshina, Y.S. Dedkov, S. Torbrügge, A. Thissen, M. Fonin, Graphene on Rh(111): scanning tunneling and atomic force microscopies studies, Appl. Phys. Lett., 100 (2012) 241606. https://doi.org/10.1063/1.4729549.
[51] M.P. Boneschanscher, J.v.d. Lit, Z. Sun, I. Swart, P.L.D.l. Vanmaekelbergh, Quantitative atomic resolution force imaging on graphene with reactive and nonreactive AFM probes, ACS Nano, 6 (2012) 10216–10221. https://doi.org/10.1021/nn3040155.
[52] S. Koch, D. Stradi, E. Gnecco, S. Barja, S.K.C. Dıaz, M. Alcamı, F.M.n.A.L.V.z.d.P.R.M.T. Glatzel, E. Meyer, Elastic response of graphene nanodomes, ACS Nano, 7 (2013) 2927–2934. https://doi.org/10.1021/nn304473r.
[53] S. Standop, O. Lehtinen, C. Herbig, G. Lewes-Malandrakis, F. Craes, J. Kotakoski, T. Michely, A.V. Krasheninnikov, C. Busse, Ion impacts on graphene/Ir(111): interface channeling, vacancy funnels, and a nanomesh, Nano Lett., 13 (2013) 1948-1955. https://doi.org/10.1021/nl304659n.
[54] J.-X. Huang, G. Csányi, J.-B. Zhao, J. Cheng, V.L. Deringer, First-principles study of alkali-metal intercalation in disordered carbon anode materials, J. Mater. Chem. A, 7 (2019) 19070-19080. https://doi.org/10.1039/C9TA05453G.
[55] P. Koskinen, S. Malola, H. Hakkinen, Self-passivating edge reconstructions of graphene, Phys. Rev. Lett., 101 (2008) 115502. https://doi.org/10.1103/PhysRevLett.101.115502.
[56] C. Uthaisar, V. Barone, J.E. Peralta, Lithium adsorption on Zigzag graphene nanoribbons, J. Appl. Phys. , 106 (2009) 113715. https://doi.org/10.1063/1.3265431.
[57] J.R. Dahn, T. Zheng, Y. Liu, J.S. Xue, Mechanisms for Lithium insertion in carbonaceous materials, Science, 270 (1995) 590-593. https://doi.org/10.1126/science.270.5236.5.
[58] E. Yoo, J. Kim, E. Hosono, H.-s. Zhou, T. Kudo, I. Honma, Large reversible Li storage of graphene nanosheet families for use in rechargeable Lithium ion batteries, Nano Lett., 8 (2008) 2277-2282. https://doi.org/10.1021/nl800957b.

[59] S. Yata, H. Kinoshita, M. Komori, N. Ando, T. Kashiwamura, T. Harada, K. Tanaka, T. Yamabe, Structure and properties of deeply Li-doped polyacenic semiconductor materials beyond C_6Li stage, Synth. Met., 62 (1994) 153-158. https://doi.org/10.1016/0379-6779(94)90306-9.
[60] S. Riikonen, A.V. Krasheninnikov, L. Halonen, R.M. Nieminen, The role of stable and mobile carbon adspecies in copper-promoted graphene growth, J. Phys. Chem. C, 116 (2012) 5802-5809. https://doi.org/10.1021/jp211818s.
[61] X. Hu, T. Björkman, H. Lipsanen, L. Sun, A.V. Krasheninnikov, Solubility of boron, Carbon, and Nitrogen in transition metals: getting insight into trends from first-principles calculations, J. Phys. Chem. Lett., 6 (2015) 3263-3268. https://doi.org/10.1021/acs.jpclett.5b01377.